

Journal of Biomedical Optics

BiomedicalOptics.SPIEDigitalLibrary.org

Terahertz pulsed spectroscopy of paraffin-embedded brain glioma

Kun Meng
Tu-nan Chen
Tao Chen
Li-guo Zhu
Qiao Liu
Zhao Li
Fei Li
Sen-cheng Zhong
Ze-ren Li
Hua Feng
Jian-heng Zhao

Terahertz pulsed spectroscopy of paraffin-embedded brain glioma

Kun Meng,^{a,b,†} Tu-nan Chen,^{a,c,†} Tao Chen,^a Li-guo Zhu,^{a,b,*} Qiao Liu,^{a,b} Zhao Li,^c Fei Li,^c Sen-cheng Zhong,^{a,b} Ze-ren Li,^{a,b} Hua Feng,^{c,*} and Jian-heng Zhao^a

^aChina Academy of Engineering Physics, Institute of Fluid Physics, Interdisciplinary Laboratory of Physics and Biomedicine, No. 64, Mianshan Road, Mianyang, Sichuan 621900, China

^bChina Academy of Engineering Physics, Terahertz Research Center, Mianyang, Sichuan 621900, China

^cThird Military Medical University, Southwest Hospital, Department of Neurosurgery, No. 30, Gaotanyan Street, Shapingba, Chongqing 400038, China

Abstract. The refractive indices, absorption coefficients, and complex dielectric constants of paraffin-embedded brain glioma and normal brain tissues have been measured by a terahertz time-domain spectroscopy (THz-TDS) system in the 0.2- to 2.0-THz range. The spectral differences between gliomas and normal brain tissues were obtained. Compared with normal brain tissue, our results indicate that paraffin-embedded brain gliomas have a higher refractive index, absorption coefficient, and dielectric constant. Based on these results, the best THz frequencies for different methods of paraffin-embedded brain glioma imaging, such as intensity imaging, coherent imaging with continuum THz sources, and THz pulsed imaging with short-pulsed THz sources, are analyzed.

© The Authors. Published by SPIE under a Creative Commons Attribution 3.0 Unported License. Distribution or reproduction of this work in whole or in part requires full attribution of the original publication, including its DOI. [DOI: 10.1117/1.JBO.19.7.077001]

Keywords: spectroscopy; terahertz; tissue diagnostics.

Paper 140175R received Apr. 11, 2014; revised manuscript received Jun. 4, 2014; accepted for publication Jun. 13, 2014; published online Jul. 7, 2014.

1 Introduction

Brain gliomas are the most common and deadly malignant brain tumors.¹ Gliomas are the leading cause of death by brain diseases in both children and adults,² and the median survival for patients with brain gliomas is a mere 12 to 15 months.³ An accurate, early clinical diagnosis of brain gliomas is crucial for patients' treatment, in which microscopic pathology is the most commonly used technique for tissue analysis. Embedding brain gliomas in paraffin is a widely used first step in microscopic pathology analysis owing to its better storage and long-term tissue morphology preservation in clinical settings.⁴ In addition, there are a large number of paraffin-embedded brain gliomas stored in medical institutions, which also provide unique opportunities for later pathological studies. More importantly, by excluding water, paraffin-embedded brain gliomas allow us to reveal the intrinsic properties of brain gliomas.

The most common method for microscopic pathology analysis of paraffin-embedded brain gliomas requires pathological markers.⁵ The marker can be visualized using appropriate staining methods with an optical microscope. This method is called a gold standard. A final diagnosis is achieved based on histopathology, immunohistochemical stains, and other methods.^{6,7} Consequently, it takes a significant amount of time and resources to obtain a reliable result. Unfortunately, experience is required to interpret paraffin-embedded brain samples, which is not an objective standard and is subject to interobserver variation or error.⁸

Therefore, an objective, label-free, quantitative analysis technique for paraffin-embedded brain glioma is required. The

terahertz (THz) spectroscopic technique, which is a novel medical imaging modality,⁹ has received a attention for its benign nature (noninvasive and nonionizing) toward humans and its high sensitivity to biomolecules^{10,11} and tissues.¹²⁻¹⁴ In recent decades, the THz spectroscopic technique has been used to identify tumors on skin,¹⁵⁻¹⁷ breast,¹⁸⁻²⁰ colon,²¹⁻²³ liver,²⁴ and other locations. All of the results show that the THz spectroscopic technique has potential for safely identifying disease in tissue samples.

Compared with normal brain tissues, brain gliomas have increased nuclear atypia, mitotic activity, florid microvascular proliferation, and necrosis,²⁵ all of which will change its THz refractive index, absorption, and scattering. Therefore, the THz spectrum of the brain glioma will be different from that of normal brain tissue. Previous studies on snap-frozen brain tissue²⁶ and fresh brain tumors²⁷ also provide preliminary experimental evidence that THz spectroscopy is able to identify brain tissue diseases. The brain tissues studied in these two studies contained an abundance of water. However, water greatly absorbs THz waves.⁹ The THz absorption reported in these experiments is primarily a result of the interstitial water content of the brain tumor and normal tissue. Most of the tissues studied by THz spectroscopy can be classified into three forms: fresh tissues,^{12,13,16} frozen tissues,²⁶ and paraffin-embedded tissues.^{23,24} The fresh tissues contain a large volume of water (THz absorption coefficient is about 240 cm⁻¹ at 1 THz),⁹ which contribute most to THz absorption in fresh tissues, while frozen tissues²⁶ and paraffin-embedded tissues^{23,24} have much lower THz absorption than that of fresh tissues by excluding water. Tumors cannot be accurately differentiated from normal brain tissue by using only the water content. As we stated previously, paraffin embedding brain gliomas is the standard method for brain pathology analysis. By excluding water, paraffin-embedded brain gliomas allow us to reveal intrinsic glioma properties in the THz spectrum.

*Address all correspondence to: Li-guo Zhu, E-mail: zhuliguo@tsinghua.org.cn; Hua Feng, E-mail: fenghua888@aliyun.com

†These authors contributed equally.

In this study, we eliminated the impact of water and obtained the THz spectra (refractive index, absorption coefficient, and complex dielectric constant) of paraffin-embedded brain gliomas, which were established by standard surgical implantation of glioma models in mice. Furthermore, the THz spectral differences between brain gliomas and normal brain tissues were obtained and analyzed in this work. Based on these results, suitable parameters and frequency components for brain glioma identification are analyzed, which may serve as a new gold standard for pathology analysis.

2 Samples and Methods

2.1 Samples

The brain tumor models for our study were glioma models from mice. GL261 cell line was obtained from American Type Culture Collection (ATCC, Manassas, Virginia). A total of 10 6-week-old specific pathogen-free level (SPF-level) C57BL/6 male mice weighing 22 ± 2 g were obtained from the Laboratory Animal Center at the Third Military Medical University and used in this study. Approval for this study was granted by the local Research Ethics Committee. The experimental procedures were approved by the Ethic Committee of Southwest Hospital, Third Military Medical University.

The animals received orthotopic transplantation of GL261-NS cells. Briefly, the mice were anesthetized with 400-mg/kg chloral hydrate by intraperitoneal injection. The cell density was adjusted to 2×10^6 cells/mL in serum-free Dulbecco's modified Eagle medium/nutrient mixture F-12 (DMEM/F12) culture medium, and then 5 μ L of the cell suspension was injected into the right caudate nucleus. The mice were placed on a stereotaxic instrument. After sterilization and skin incision, a 3-mm-diameter hole was made with a microelectrical drill on the skull at a position of 1.4-mm anterior from the anterior fontanel and 2.0-mm lateral from the sagittal suture. Stereotaxic coordinates were taken from bregma and dura mater according to the mouse brain atlas.²⁸ Mice were maintained for 20 days. The brains of euthanized mice were collected and fixed in 10% formalin for 24 h. Then, the whole formalin-fixed mouse brain was washed by a current water, dehydrated using graded ethanol [0% ethanol for 1 h, 95% ethanol (95% ethanol/5% methanol) for 1 h, first absolute ethanol for 1 h, second absolute ethanol for 1.5 h, third absolute ethanol for 1.5 h, and fourth absolute ethanol for 2 h], vitrification by xylene (first xylene for 1 h, second xylene for 1 h), and infiltrated with wax (first wax at 58°C for 1 h, second wax at 58°C for 1 h). The infiltrated tissues were then embedded into wax blocks. The paraffin-embedded tissues were made of paraffin sections following the traditional medical methodology.²⁹ Then, they were cut into slices with the thickness between 1 and 2.5 mm (hundreds of times thicker than the classical paraffin section in order to increase THz absorption), which helped to reduce the etalon effect. Both sides of the samples were polished and kept parallel (with roughness < 50 μ m). Both cancerous and healthy tissues were removed from each mouse, producing a total of 20 samples.

2.2 Experimental Methods

The experimental setup used in this study is a transmission THz time-domain spectroscopy (TDS) system (Fig. 1), whose THz emitter is a photoconductive antenna with an electrode

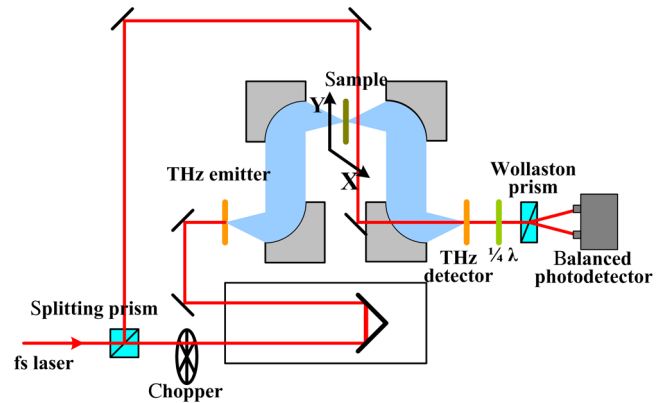


Fig. 1 Schematic representation of the terahertz time-domain spectroscopy system.

distance of 50 μ m. The detector is based on a 1-mm-thick ZnTe crystal.

In our setup, a femtosecond fiber laser (MenloSystem Inc., Martinsried, Germany, F-780A), which operates with a 100-MHz repetition rate, is used to provide 100-fs laser pulses with a central wavelength of 780 nm. The laser pulses are split into a pump beam and a probe beam by a beam splitter. The pump beam is incident on the photoconductive emitter to produce electron-hole pairs, which are then accelerated by a biased electric field. According to Maxwell's theory, these accelerated electron-hole pairs will generate a transient electric field and emit a transient electromagnetic wave. Because the duration of the excited laser pulse is 100 fs and the lifetime of the photoexcited carriers in the antenna substrate (low-temperature GaAs) is about 360 fs, the duration of the transient electromagnetic wave is on the picosecond order, lying in the THz band. The THz pulses are collimated to the sample by a pair of silver-coated off-axis parabolic mirrors, and then the pulses carrying information about the samples are guided to the THz detector by another pair of off-axis parabolic mirrors, changing the refractive index of ZnTe. This change will be encoded by the probe beam, which reaches the crystal synchronously, and will be detected by a balanced photodetector. After lock-in amplification, the signal will be recorded, and the waveform of the THz pulse will be measured by time-domain sampling. In order to remove the effect of water vapor, a sample chamber, which can be purged with nitrogen, was used to reduce the relative humidity down below 5% during the whole experiment. Moreover, each sampled data point in the THz pulse is measured five times and averaged to increase the signal-to-noise ratio.

To obtain the sample spectra, both the reference pulse, which is measured in the absence of the sample, and the sample pulse, which is measured when a sample is positioned in the focal point of the THz wave (Fig. 1), were measured as shown in Fig. 2(a). Then, a fast Fourier transform is used to obtain the frequency-domain electric field, which is shown in Fig. 2(b) demonstrating that the maximum signal-to-noise ratio of the system surpasses 2000. As the THz wave propagates from the THz emitter to the detector, it could be described in the frequency-domain as

$$E_{\text{ref}}(\omega) = E_0(\omega) \exp\left(-i\omega t + i\frac{\omega}{c}l\right), \quad (1)$$

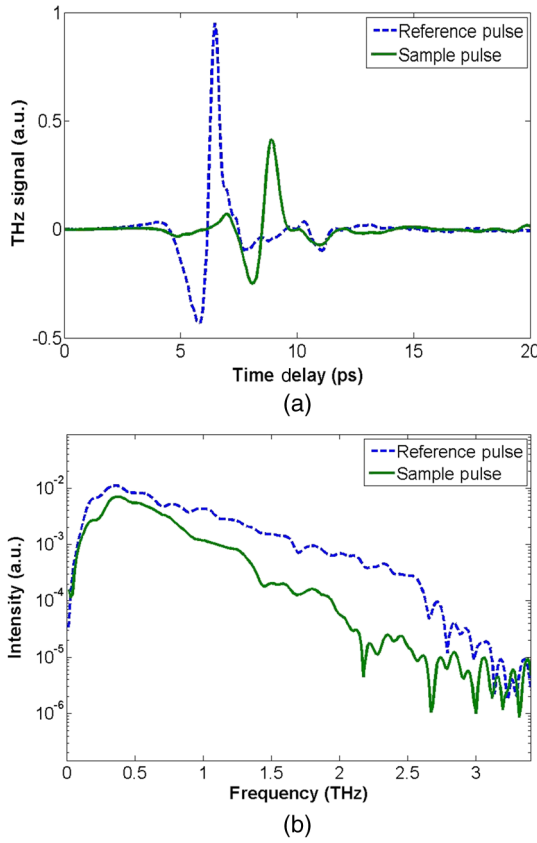


Fig. 2 Measured reference pulse and sample pulse: (a) time-domain and (b) frequency-domain.

$$\begin{aligned}
 E_{\text{sam}}(\omega) &= E_0(\omega) \frac{2}{N(\omega)+1} \exp \left[-i\omega t + i \frac{n(\omega)\omega}{c} d + i \frac{\omega}{c} (l-d) \right] \\
 &\times \exp \left[-\frac{\kappa(\omega)}{c} d \right] \frac{2N(\omega)}{N(\omega)+1} \\
 &\times \sum_{k=0}^{\infty} \left\{ \left[\frac{N(\omega)-1}{N(\omega)+1} \right]^2 \cdot \exp \left[i \frac{2n(\omega)\omega}{c} d - \frac{2\kappa(\omega)}{c} d \right] \right\}^k, \quad (2)
 \end{aligned}$$

where E_0 is the original THz pulse emitted by the photoconductive antenna, l is the full path that the THz wave travels, d is the thickness of the sample, and $N(\omega) = n(\omega) + i\kappa(\omega)$ is the complex refraction of measured sample, in which $n(\omega)$ is the refractive index, and $\kappa(\omega)$ is the extinction coefficient.

To calculate the refractive index and the absorption coefficient, the following division will be performed

$$S(\omega) = \frac{E_{\text{sam}}(\omega)}{E_{\text{ref}}(\omega)}. \quad (3)$$

Our paraffin-embedded samples are made by a precise medical-standard slicer, whose thicknesses were then measured by a vernier micrometer. The refractive index and the extinction coefficient can be derived using numerical methods.³⁰ When calculating refractive index and absorption coefficient, we also considered samples' thickness variation, which contribute to the error bar in THz refractive index and absorption coefficient (see Figs. 3 and 4). Then, the absorption coefficient can be calculated as follows:

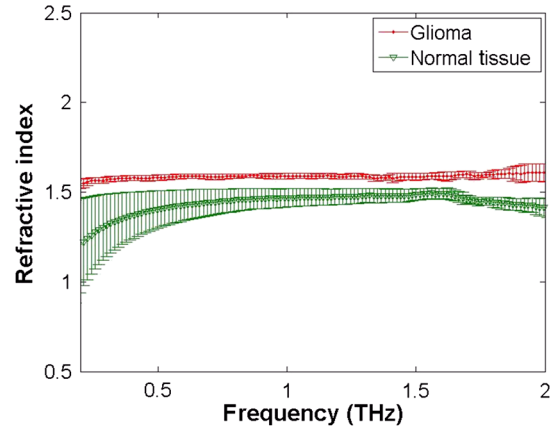


Fig. 3 Refractive indices of glioma and normal tissue.

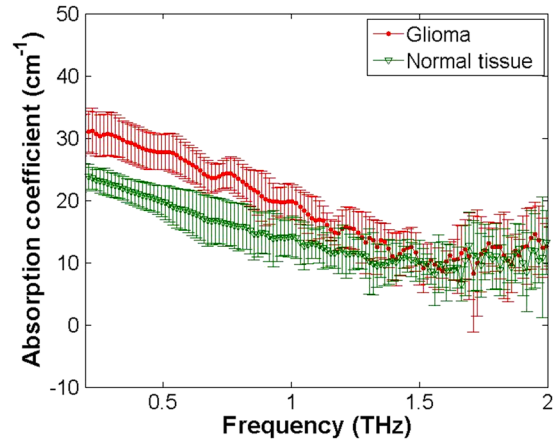


Fig. 4 Absorption coefficient of glioma and normal tissue (one order of magnitude lower absorption coefficient in paraffin-embedded brain tissues than these of fresh tissues^{12,13,16} is mainly because water is excluded in the former samples, which is the intrinsic properties of brain tissues in THz range).

$$\alpha(\omega) = \frac{2\kappa(\omega)\omega}{c}. \quad (4)$$

3 Results and Discussion

Twenty paraffin-embedded brain samples, which include 10 brain gliomas with the same illness and 10 normal brain tissues, were tested in our experiments, and three different spots on each sample were measured. The preparation processes, especially the lesion severity, of the 10 pieces of brain gliomas are the same. To this extent, all the samples and measured spot are “identical” and of the same refractive index and absorption coefficient in the THz range. But biology is diverse; the statistics diversity leads to difference in our experimental results. Also, the statistics diversity is shown as statistics error bars in the THz spectrum of refractive index and absorption coefficient (see Figs. 3 and 4). The error bars are derived from the standard error of the mean. Therefore, Figs. 3 and 4 display 95% confidence intervals.

As shown in Fig. 3, there is a clear difference in the refractive indices between the brain gliomas and the normal brain tissues. The refractive indices of glioma are stable at about 1.6 THz over

the measured THz range from 0.2 to 2.0 THz. On the other hand, the refractive indices of normal tissue display a slight increase in the low-frequency range before 1.5 THz and a slight decrease for higher frequencies. The mean values of the refractive indices for normal tissue are between 1.2 and 1.5 THz.

Regarding the absorption coefficient, a distinct difference between the brain gliomas and the normal brain tissues occurred only at frequencies below 1 THz, as shown in Fig. 4. At higher frequencies, the error bars overlapped, and it was difficult to distinguish the difference between gliomas and normal tissues.

In our experimental results, both the refractive indices and the absorption coefficient of gliomas are larger than those of normal tissue. Because our specimens are dehydrated, these differences are not caused by the water content. Consequently, our results reveal differences in the cell components and morphology between gliomas and normal brain tissues. Different cell components may cause different THz responses by absorption, dispersion, and reflection, while different morphologies may cause different THz responses by scattering. Identifying the contribution of each mechanism requires an additional medical analysis.

To be clear, we calculated the differences in the refractive indices and absorption coefficient spectra between gliomas and normal brain tissues (Fig. 5). In the frequency range from 0.2 to 1.5 THz, the difference in the refractive indices decreases as the frequency increases, while the difference

increases for increasing frequency in the 1.5- to 2.0-THz range. On the other hand, the difference in the absorption coefficient spectra is only obvious below 1 THz, especially at frequencies of 0.3, 0.55, and 0.76 THz as shown in Fig. 5(b).

The dielectric constant is also an important physical parameter and can be derived by $\epsilon = \epsilon_r + i\epsilon_i = (n + ik)^2$. Figure 6 shows the calculated dielectric constant results. As we can see, differences between gliomas and normal brain tissues are apparent for both the real and imaginary parts of the dielectric constant.

For imaging applications, the imaging contrast is an important parameter, which depends on the relative spectral difference rate between gliomas and normal tissues. Higher relative spectral difference rates produce clearer images. The relative rate can be calculated from the difference between the glioma spectra and the normal tissue spectra divided by the normal tissue spectra. For unstable biomaterial parameters, such as those shown in Figs. 3–6, the error bars cannot be ignored, and the confidence intervals must be considered when calculating the difference between spectra. In this study, we employ a strict standard for evaluating the imaging contrast. The differences between spectra were obtained by subtracting the spectral value of the upper edge of the normal tissue confidence interval from the spectral value of the lower edge of the glioma confidence interval. Furthermore, the relative rates of all parameters discussed were calculated as shown in Fig. 7.

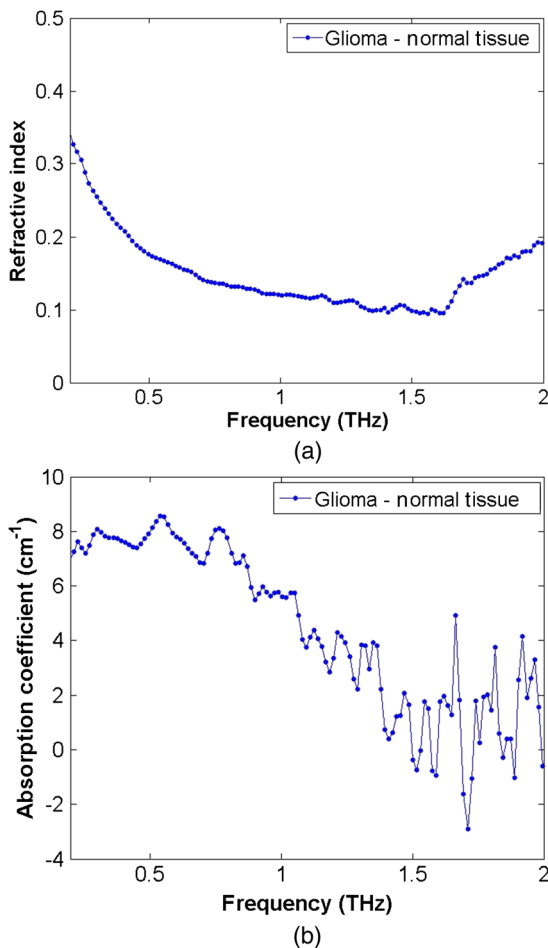


Fig. 5 (a) Refractive index and (b) absorption coefficient difference between glioma and normal brain tissue.

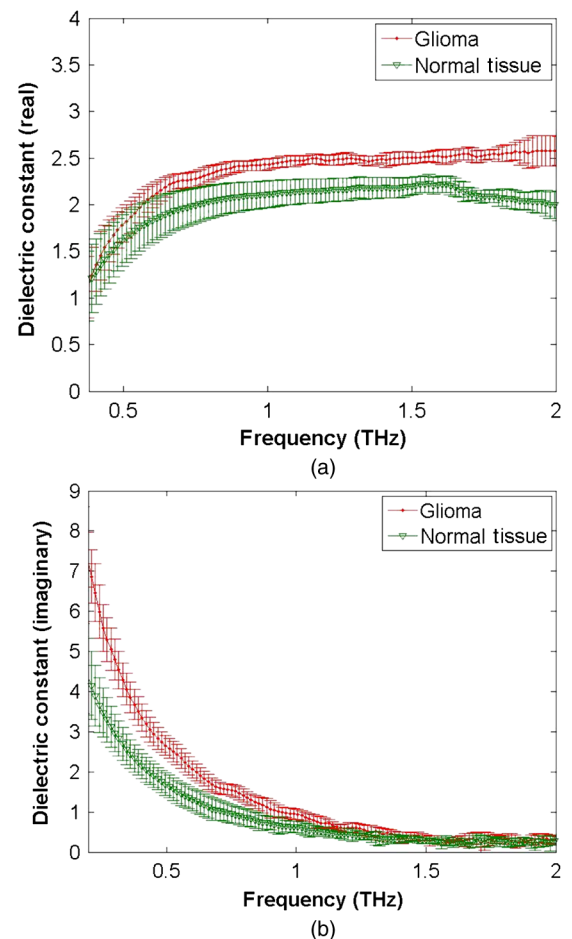


Fig. 6 Dielectric constants of glioma and normal brain tissue: (a) real part and (b) imaginary part.

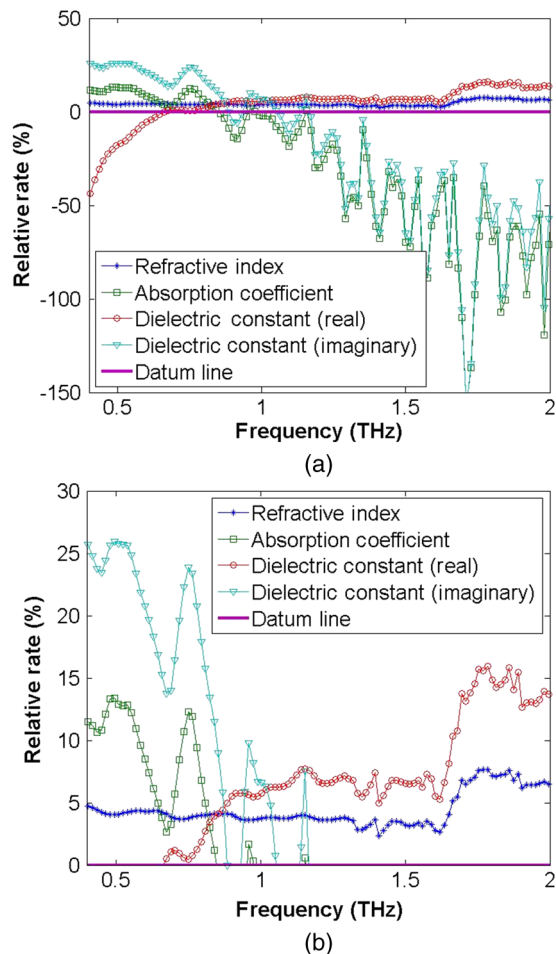


Fig. 7 Relative rates of the refractive index, absorption coefficient, and dielectric constant. (a) The full curves and (b) the positive portions of the curves.

To define the imaging contrast, Fig. 7(a) shows the relative rates for the refractive index, absorption coefficient, and dielectric constant. As shown in Fig. 7(a), the rates may be negative, which is caused in our method when the error bars overlap. In this situation, it is impossible to distinguish glioma from normal tissue. We are only concerned with positive relative rates. To be clear, the positive portions of the curves are illustrated in Fig. 7(b). For frequencies below 1.0 THz, the absorption coefficient and the imaginary part of the dielectric constant show better contrast. On the other hand, the refractive index and the real part of the dielectric constant show better contrast in the 1.7- to 2.0-THz range.

Of all four parameters, the imaginary part of the dielectric constant provides the largest contrast below 1.0 THz and reaches a relative rate of about 26% at 0.55 THz. In the 1- to 2-THz frequency range, the real part of the dielectric constant provides a better standard for distinguishing gliomas from normal tissues. According to these results, imaging based on the complex dielectric constant would provide the most reliable method. THz pulse imaging, based on THz-TDS spectroscopy, is the most powerful THz imaging technology, capable of obtaining all four parameters mentioned above. According to our results, THz pulse imaging can potentially obtain a clear image of paraffin-embedded brain gliomas.

On the other hand, when it is not necessary to obtain all information for a particular sample, continuous-wave THz imaging is a time-saving diagnostic technique, which has been widely studied in biomedical applications.^{31,32} Moreover, if suitable frequency components are utilized, continuous-wave imaging may provide a useful result.³³ Our results should also be valuable for distinguishing between gliomas and normal brain tissues in continuous-wave THz imaging. There are two main methods of continuous-wave imaging: coherent imaging, which depends on the difference of the refractive indices, and intensity imaging, which depends on the difference of the absorption coefficients. As shown in Fig. 7(b), the relative rate of the refractive index is stable in the low-frequency range and shows some increase in the 1.7- to 2.0-THz frequency range. Both of these frequency ranges are suitable for coherent imaging. Moreover, the absorption difference shows two peaks at 0.55 and 0.76 THz, and these two frequency components are suitable for intensity imaging.

4 Conclusion

In summary, we successfully measured the refractive index, absorption coefficient, and complex dielectric constant of paraffin-embedded brain gliomas and normal brain tissues in the 0.2- to 2.0-THz frequency range. According to our results, gliomas had a higher refractive index, absorption coefficient, and dielectric constant than normal brain tissues. We further discussed the imaging contrast. From our analysis, the dielectric-constant-based imaging may give the best contrast, and it is very suitable for THz pulsed imaging. THz waves with higher frequencies, such as those in the 1.7- to 2.0-THz range, are suitable for coherent imaging, while waves with lower frequencies, especially those at 0.55 and 0.76 THz, are suitable for intensity imaging. These results demonstrate that THz technology has the potential to distinguish gliomas from normal brain tissues and are valuable for THz imaging of paraffin-embedded brain glioma.

Acknowledgments

This work was supported by NSAF (Grant No. U1230128), NSFC (Grant No. 61205100), Key Foundation of CAEP (Grant No. 2012A0401016), CPSF (Grant No. 2014M552542XB), NSF of Chongqing (Grant No. cstc2012jjB0081), and the Incubation Foundation of Interdisciplinary Laboratory of Physics and Biomedicine.

References

1. E. G. Van Meir et al., "Exciting new advances in neuro-oncology: the avenue to a cure for malignant glioma," *CA Cancer J. Clin.* **60**(3), 166–193 (2010).
2. J. C. Buckner et al., "Central nervous system tumors," *Mayo Clin. Proc.* **82**(10), 1271–1286 (2007).
3. P. Y. Wen and S. Kesari, "Malignant gliomas in adults," *N. Engl. J. Med.* **359**(5), 492–507 (2008).
4. D. W. Mahoney et al., "Quality assessment metrics for whole genome gene expression profiling of paraffin embedded samples," *BMC Res. Notes* **6**(33), 1–11 (2013).
5. M. Jansen, S. Yip, and D. N. Louis, "Molecular pathology in adult gliomas: diagnostic, prognostic, and predictive markers," *Lancet Neurol.* **9**(7), 717–726 (2010).
6. T. Rüdiger et al., "Quality assurance in immunohistochemistry: results of an interlaboratory trial involving 172 pathologists," *Am. J. Surg. Pathol.* **26**(7), 873–882 (2002).
7. H. Mohan, *Pathology Practical Book*, Jaypee Brothers Medical Publishers Ltd, New Delhi, India (2007).

8. J. M. Crawford, "Original research in pathology: judgment, or evidence-based medicine?," *Lab. Invest.* **87**(2), 104–114 (2007).
 9. P. H. Siegel, "Terahertz technology in biology and medicine," *IEEE Trans. Microwave Theory Tech.* **52**(10), 2438–2447 (2004).
 10. M. Tonouci, "Cutting-edge terahertz technology," *Nat. Photonics* **1**(2), 97–105 (2007).
 11. Y. Sun et al., "A promising diagnostic method: terahertz pulsed imaging and spectroscopy," *World J. Radiol.* **3**(3), 55–65 (2011).
 12. G. J. Wilmink et al., "Development of a compact terahertz time-domain spectrometer for the measurement of the optical properties of biological tissues," *J. Biomed. Opt.* **16**(4), 047006 (2011).
 13. I. Echchgadda et al., "Using a portable terahertz spectrometer to measure the optical properties of *in vivo* human skin," *J. Biomed. Opt.* **18**(12), 120503 (2013).
 14. E. Pickwell et al., "Simulating the response of terahertz radiation to basal cell carcinoma using ex vivo spectroscopy measurements," *J. Biomed. Opt.* **10**(6), 064021 (2005).
 15. R. M. Woodward et al., "Terahertz pulse imaging in reflection geometry of human skin cancer and skin tissue," *Phys. Med. Biol.* **47**(21), 3853–3863 (2002).
 16. R. M. Woodward et al., "Terahertz pulse imaging of ex vivo basal cell carcinoma," *J. Invest. Dermatol.* **120**(1), 72–78 (2003).
 17. E. Pickwell et al., "In vivo study of human skin using pulsed terahertz radiation," *Phys. Med. Biol.* **49**(9), 1595–1607 (2004).
 18. J. F. Anthony et al., "Terahertz pulsed imaging of human breast tumors," *Radiology* **239**(2), 533–540 (2006).
 19. E. Pickwell MacPherson, A. J. Fitzgerald, and V. P. Wallace, "Breast cancer tissue diagnosis at terahertz frequencies," *Proc. SPIE* **8221**, 82210M (2012).
 20. H. Chen et al., "Performance of THz fiber-scanning near-field microscopy to diagnose breast tumors," *Opt. Express* **19**(20), 19523–19531 (2011).
 21. F. Wahaia et al., "Detection of colon cancer by terahertz techniques," *Proc. SPIE* **8006**, 800130 (2011).
 22. C. B. Reid et al., "Terahertz pulsed imaging of freshly excised human colonic tissues," *Phys. Med. Biol.* **56**(14), 4333–4353 (2011).
 23. F. Wahaia et al., "Detection of colon cancer by terahertz techniques," *J. Mol. Struct.* **1006**(1–3), 77–82 (2011).
 24. T. Enatsu et al., "Terahertz spectroscopic imaging of paraffin-embedded liver cancer samples," in *2007 Joint 32nd Int. Conf. on Infrared and Millimeter Waves and the 15th Int. Conf. on Terahertz Electronics*, pp. 557–558, IEEE, Cardiff (2007).
 25. P. Wesseling, J. M. Kros, and J. W. M. Jeuken, "The pathological diagnosis of diffuse gliomas: towards a smart synthesis of microscopic and molecular information in a multidisciplinary context," *Diag. Histopathol.* **17**(11), 486–494 (2011).
 26. G. M. Png et al., "Terahertz spectroscopy of snap-frozen human brain tissue: an initial study," *Electron. Lett.* **45**(7), 343–344 (2009).
 27. S. J. Oh et al., "Terahertz pulse imaging of fresh brain tumor," in *2011 36th Int. Conf. on Infrared, Millimeter and Terahertz Waves (IRMMW-THz)*, pp. 1–2, IEEE, Houston, TX (2011).
 28. K. B. J. Franklin and G. Paxinos, *The Mouse Brain in Stereotaxic Coordinates*, Academic Press, San Diego (1997).
 29. D. K. Wright and M. M. Manos, "Sample preparation from paraffin-embedded tissues," *PCR Protoc.: Guide Methods Appl.* **19**, 153–159 (1990).
 30. W. Withayachumnankul et al., "Material parameter extraction for terahertz time-domain spectroscopy using fixed-point iteration," *Proc. SPIE* **5840**, 221–231 (2005).
 31. E. Pickwell and P. Wallace, "Biomedical applications of terahertz technology," *J. Phys. D* **39**(17), R301–R310 (2006).
 32. K. Humphreys et al., "Medical applications of terahertz imaging: a review of current technology and potential applications in biomedical engineering," in *Proc. of the 26th Annual Int. Conf. of the IEEE EMBS*, pp. 1302–1305, IEEE, San Francisco, CA (2004).
 33. N. Karpowicz et al., "Comparison between pulsed terahertz time-domain imaging and continuous wave terahertz imaging," *Semicond. Sci. Technol.* **20**, S293–S299 (2005).
- Kun Meng** received his BS degree in physics from Shandong University in 2008 and his MS degree in optics from CAEP in 2011. He is an assistant professor at the Institute of Fluid Physics, China Academy of Engineering Physics. His current research interests include terahertz spectroscopy and imaging.
- Tu-nan Chen** received his PhD degree in neurosurgery from The Third Military Medical University in 2012. He is an assistant professor. His current research interests include brain tumor diagnosis and brain mapping.
- Biographies of the other authors are not available.